Major Improvement in the Cycling Ability of Pseudocapacitive Vanadium Nitride Films for Micro-Supercapacitor

Aiman Jrondi, Gaëtan Buvat, Francisco de La Pena, Maya Marinova, Marielle Huvé, Thierry Brousse, Pascal Roussel, Christophe Lethien

Major improvement in the cycling ability of pseudocapacitive vanadium nitride films for micro-supercapacitor

Aiman Jrondi[1,2,3], Gaetan Buvat[1,2,3], Francisco De La Pena[4], Maya Marinova[5], Marielle Huvé[2], Thierry Brousse[3,6*], Pascal Roussel[2*] and Christophe Lethien[1,3,7*]

[1] Institut d'Electronique, de Microélectronique et de Nanotechnologies, Université de Lille, CNRS, Université Polytechnique Hauts-de-France, UMR 8520 - IEMN, F-59000 Lille, France

[2] Unité de Catalyse et de Chimie du Solide (UCCS), Université de Lille, CNRS, Centrale Lille, Université d'Artois, UMR 8181 – UCCS, F-59000 Lille, France

[3] Réseau sur le Stockage Electrochimique de l'Energie (RS2E), CNRS FR 3459, 33 rue Saint Leu, 80039 Amiens Cedex, France

[4] Unité Matériaux et Transformations, Université de Lille, CNRS, UMR 8207, Lille France

[5] Université de Lille, CNRS, INRAE, Centrale Lille, Université d'Artois, FR 2638, IMEC – Institut Michel-Eugène Chevreul, F-59000 Lille, France

[6] Nantes Université, CNRS, Institut des Matériaux de Nantes Jean Rouxel, IMN, F-44000 Nantes, France

[7] Institut Universitaire de France (IUF), Saint-Michel 103, 75005, Paris, France

*Correspondence to: christophe.lethien@univ-lille.fr, thierry.brousse@univ-nantes.fr & pascal.roussel@univ-lille.fr

KEYWORDS: Vanadium nitride, sputtering, pseudocapacitance, cycling stability, high rate, ageing

ABSTRACT:

Vanadium nitride film made from thin film deposition technique is a promising electrode material for micro-supercapacitor's application owing to its high electrical conductivity and high volumetric and surface capacitances values in aqueous electrolyte. Nevertheless, the cycling stability has to be improved to deliver good capacitance during a large number of cycles. Here we show that vanadium nitride films made by magnetron sputtering deposition method exhibit remarkable cycling stability (high capacitance retention value after 150 000 cycles), ultra-high rate capability (75 % of the initial capacitance at 1.6 $V.s^{-1}$), while providing high surface capacitance values (~ 1.4 $F.cm^{-2}$) and very low ageing of the VN electrodes (no loss of the performance after 13 months). Additionally, new findings regarding the location of vanadium oxides species responsible for the charge storage mechanism in pseudocapacitive VN films are revealed by transmission electron microscopy EELS (electron energy loss spectroscopy) analyses at the nanoscale.

Table of Contents

Sputtered vanadium nitride film as an efficient electrode material and current collector for micro-supercapacitor was optimized to deliver high capacitance, high cycling stability, low ageing and high rate capability. The charge storage process occurring at the surface of a very thin layer of vanadium oxides within the VN film was deeply investigated and this study unveils for the first time the position of oxide species responsible for the pseudocapacitive behavior of the electrode.

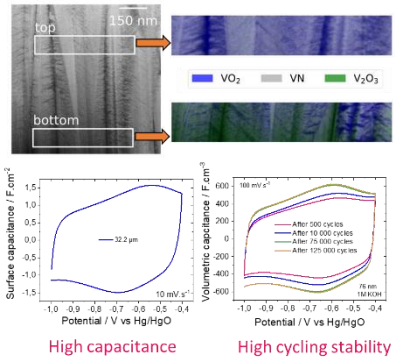

High capacitance High cycling stability

INTRODUCTION

Micro-supercapacitors (MSC) constitute a class of electrochemical energy storage device with limited footprint surface and where all materials that make up the MSC are deposited on a substrate by deposition methods allowing a fine control of film quality and thickness[1–3]. When talking about MSC, the total thickness of the stacked films is below 50 µm (substrate ~ 500 µm) and the footprint surface (< 1 cm^2) is controlled by etching technique (top down approach: chemical or plasma etching methods) or localized growth of the active material on current collector (bottom up approach: ink jet printing, electrodeposition).

The first MSC was made in 2001 by Yoon *et al*: the magnetron sputtering deposition technique was selected to stack electrode material and solid electrolyte on a silicon wafer giving rise to Si / SiO_2 / RuO_2 / LiPON / RuO_2 stacked layers[4,5]. The capacitance retention of this MSC was restricted (< 1000 cycles) and the rate capability was limited owing to the low ionic conductivity of the LIPON solid electrolyte[6–8] (σ_{ionic} ~ 10^{-6} $S.cm^{-1}$ at room temperature) but the triangular shape of the Galvanostatic Charge – Discharge plot confirmed the pseudocapacitive properties of the RuO_2 / LIPON / RuO_2 MSC. More than twenty years after this first demonstration, it must be said that there is still no commercially available MSC while applications where small connected sensors requiring energy autonomy to measure and share data in the field of Internet of Things (IoT) paradigm are numerous (structural health monitoring, environmental monitoring, animal tracking…). Various technological locks have to be solved to improve the Technological Readiness Level (TRL) of MSC before arriving at a mature product that can be sold to address these markets. The 1st limitation deals with the use of a solid electrolyte exhibiting a high ionic conductivity at room temperature. Hydrogels[9,10] where aqueous electrolyte (H_2SO_4, KOH, Na_2SO_4…) are trapped in a

polymer matrix (PVA, PVDF…) could be an issue but they suffer from water evaporation limiting the cycling stability. An interesting alternative concerns the use of ionogels where ionic liquids are confined in a porous host matrix[11–13]: in that case, the gel does not suffer from water evaporation and the ionic conductivity of the ionogel corresponds approximately to that of the pure ionic liquid[11]. Several demonstration where ionogel technology is proposed as the solid electrolyte of MSC have been published[13–16] recently to highlight this promising technology. Nevertheless, the footprint surface of the solid electrolyte has to be limited to the one of the electrode materials: in that case, ionogel solid electrolyte with photopatternable capabilities[17] compatible with microfabrication method or ionogel deposited by inkjet printing[18] on electrode materials are the most advanced method to fulfil the surface requirement for MSC applications.

The 2nd technological bottleneck lies with the use of electrode materials made by deposition methods with homogeneous thickness, performance and reproducibility on large scale substrate (3'' or 4'' Silicon wafer as an example). Carbon electrodes can be fabricated by electrophoretic deposition[19], inkjet printing[20] or chlorination of Carbide-derived carbon films[1,21]. The electrosorption charge storage process of porous carbon material in organic electrolyte led to low surface capacitance value (< 100 mF.cm^{-2}) but the working potential window was close to ~ 3V. To improve the capacitance value (> 1 F.cm^{-2}), an attractive solution consists in depositing thin film of pseudocapacitive materials operating in aqueous electrolyte. Fast redox reactions occurring at the surface or near the surface of a pseudocapacitive material in aqueous electrolyte provides higher capacitance than nanoporous carbon electrodes. Pseudocapacitance is used to explain the charge storage mechanism arising from fast redox reactions with no phase transformation of the electrode material. Transition

metal oxide such as ruthenium dioxide (RuO_2) [22–25] or manganese dioxide (MnO_2) [26,27] were the main investigated electrode materials for planar or 3D micro-supercapacitors[14,15,28–35] when considering these materials deposited in a thin film configuration. In that case, MnO_2 or RuO_2 films are deposited using aqueous solution processing methods – giving rise to a hydrous form – where the morphology, the thickness and the performance of the electrode could be tuned with the deposition parameters (pH, T°, potential, type of the deposition process, composition…). The capacitance value (and the electrical conductivity) is also related to the amount of water (n) in $RuO_2.nH_2O$ or $MnO_2.nH_2O$ involved in the charge storage mechanism. While the performance of pseudocapacitive oxide films made from aqueous solution processing method are very interesting, it would be difficult to obtain homogenous deposition on large-scale substrate if mass production is scheduled on pilot production line. In that case, thin film deposition methods under vacuum have to be investigated but synthesizing hydrous ruthenium dioxide or manganese dioxide films is difficult due to the under vacuum deposition process. A new class of pseudocapacitive electrode materials is currently investigated as efficient thin film electrode for MSC since the discovery of nanostructured vanadium nitride particles[36] by Choi *et al* and the demonstration of Mo_xN film[37] as a pseudocapacitive material in aqueous electrolyte by Conway *et al*. Chromium nitride[38], tungsten nitride[39], titanium nitride[40] and vanadium nitride[17,41–44] were thus investigated as thin film electrode material for MSC applications. The areal capacitance of CrN (2.4 µm-thick), W_2N (7.9 µm-thick), TiN (2.2 µm-thick) were close to ~86, 550, 18 $mF.cm^{-2}$ respectively[38–40] and the capacitance retention was investigated but rarely above 20 000 cycles. While high capacitance value (~ 1.2 $F.cm^{-2}$) was recently demonstrated by our group with sputtered vanadium nitride (VN) films deposited on Si wafer, the capacitance retention was limited close to

75 % after 50 000 cycles[43] despite the use of suitable electrochemical conditions proposed by D. Bélanger *et al* in 2016 for such electrode materials[41]. The electrochemical performance of sputtered VN films were evaluated in 1M KOH between -1 and -0.4 V vs HgO. Taking into account a symmetric configuration, the cell voltage of VN // VN MSC was only limited to 0.6 V. Recently[35], we proposed to move from a VN // VN symmetric MSC to a VN // RuO_2 asymmetric topology operating in 1M KOH. As a result, the cell voltage of the MSC was extended up to 1.15 V taking into account sputtered VN film as the negative electrode (between -1 up to -0.4 V vs Hg/HgO) and electrodeposited RuO_2 film as the positive electrode (between -0.4 up to -0.15 V vs Hg/HgO). Vanadium nitride is also an attractive solution as an electrode material for Na-ion storage devices[45]. From cycling stability and ageing point of views, it is mandatory to improve the film performance to reach higher capacitance retention while limiting the ageing of the electrode materials. Additionally, we unveiled the charge storage process in sputtered vanadium nitride films recently[43] where thin layer of vanadium oxides (mixing of V_2O_3 and VO_2) surrounding the vanadium nitride are responsible of the fast redox reactions occurring within the films. Here we demonstrate that sputtered vanadium nitride films can be tuned to maximize both the cycling stability (high capacitance retention value after 150 000 cycles) and the rate capability (75 % of the initial capacitance at 1.6 $V.s^{-1}$), while providing high surface capacitance values (~ 1.4 $F.cm^{-2}$) and very low ageing of the VN electrodes (no loss of the performance after 13 months). New findings regarding the location of vanadium oxides species responsible for the charge storage mechanism in pseudocapacitive VN films are proposed. Taking benefit from high electrical conductivity (> 4000 $S.cm^{-1}$) and very interesting electrochemical performance, this is the first time that such results are

reported for vanadium nitride film acting as efficient pseudocapacitive electrodes and current collector for micro-supercapacitors.

RESULTS AND DISCUSSION

The general strategy used in this manuscript to maximize and stabilize the electrochemical performance of vanadium nitride pseudocapacitive electrode is depicted in **fig. 1**. Previous papers[17,42,43] from our group on sputtered VN films showed how maximizing the areal capacitance while keeping the capacitance retention close to ~ 70 % after 50 000 cycles. Even if the cycling conditions were similar to those recommended by D. Bélanger *et al* (for VN thin films made from magnetron sputtering method)[41], the obtained capacitance retention value are however not sufficient from the cycling stability point of view for “real-life” MSC applications. This paper aims at proposing a pertinent strategy to make VN films with high cycling stability, low ageing, high rate capability, while keeping remarkable surface capacitance value. To reach this goal, the deposition parameters (pressure, gas ratio, thickness) of the VN films were carefully tuned and studied as illustrated in **fig. 1**.

In the present paper, in a first step, while it was fixed at 17 % in our previous papers[17,42–44], we propose to finely tune the N_2 content in the total gas (N_2 / (N_2+Ar), in %) from 5 up to 100 % while keeping constant the other deposition parameters (Room temperature, deposition pressure = 10^{-2} mbar, DC power = 1.85 W.cm^{-2}, deposition time = 45 minutes). In a second step, the influence of the pressure will be investigated, and finally the thickness. Scanning Electron Microscope analyses made on the VN films are given **fig. 2a** and **SI1a**. Top view images reveal a progressive shift of the film morphology from pyramidal-shape (at low N_2 content) to cauliflower-shape (at high N_2 content). These observations are consistent with our previous studies (N_2 content ~ 17 %) and with the paper[41] from D. Bélanger *et al* focused on sputtered VN films deposited with N_2 content ~ 8 %. From cross-sectional analyses shown in **fig. SI1a**, the morphology of the films is found to be columnar – following a feather-like

growth morphology – with large spacing and void between and within the columns at low N_2 content. The increasing of the N_2 content in the gas mixture produces then a densification process of the VN films, resulting from the nitridation of the metallic vanadium sputtering target. Indeed, when a threshold of N_2 flow is reached, the excess of N_2 reacts with the target surface (poisoning effect) and the argon ions impinging the V-N layer of the target remove this layer. At low N_2 content in the total gas, most of the nitrogen gas is kept by the vanadium atoms and deposited on the substrate and the target surface is kept purely metallic. The combination of these two different processes controls the film densification. Consequently, the evolution of the film density, film thickness and electrical conductivity are important parameters to follow. There evolutions are plotted in **fig. 2b**. On one hand, the thickness of the sputtered films is progressively reduced when the N_2 flow is increased (constant deposition time) due to previously evoked target poisoning effect. The nitridation of the metallic target by the nitrogen gas within the sputtering reactor induces a reduction of the vanadium yield and thus a lower thickness. On the other hand, the film density and the electrical conductivity follow the opposite trend. The film densification occurs when the nitrogen content in the total gas is increased thus resulting in the reduction of defects or voids. In that case, a significant enhancement of the electrical conductivity is observed increasing from 400 (at low N_2 content) up to ~ 3700 $S.cm^{-1}$ (at high N_2 content).

Fig. SI1b gives representative diffractograms with various N_2 ratios in the plasma (from 10% to 100%). First, the appearance of the (200) peak for highest N_2 contents (from 80% to 100%) is indicating a change in the preferred orientation in the film. Secondly, if we zoom on the (111) peak position, a clear variation is observed (**fig. SI1c**), leading to the cell-parameters evolution given in **fig. 2c**. Indeed, the cell parameter (considering a Fm-3m cubic symmetry) is decreasing from 10% to 30%, and thus

increasing for higher content. This peculiar behavior can be attributed to a competition between the expected one for a classical solid-solution (i.e a continuous increase with the N_2 content) with a mechanical stress issue, classically observed for low N_2 content[46]. Indeed, it has been reported that the residual stress is maximum for lowest N_2 content and is correlated to preferred orientation. We can thus propose, in these conditions (pressure = 10^{-2} mbar, deposition at room temperature, no bias, DC power = 1.85 W.cm^{-2}), that stress is predominant for lower N_2 content and that, for higher N_2 ratios, the film is more relaxed and follow a more classical behavior, approaching the behavior of bulk free powder. This hypothesis is in good agreement with the evolution of the cell parameter that, for high N_2 contents, is approaching the theoretical expected value reported for powder (a = 4.139 Å, PDF number 35-0768). The crystallinity of the film is also impacted, as can be observed with the evolution of the Full Width at Half Maximum (FWHM, see **Fig. SI1d**) which is decreasing with the N_2 content, and could be related to a strain relaxation.

The electrochemical properties of sputtered vanadium nitride films were evaluated regarding the nitrogen content in aqueous electrolyte (1M KOH) and EMIM-TFSI ionic liquid. The aim of these measurements is to extract and compare the pseudocapacitive contribution (measured in 1M KOH) *vs* the electrical double layer (EDL) capacitance, this latter value being issued from the electrosorption of ions coming from the ionic liquid in the VN films. The CV plots at 5 mV.s^{-1} are depicted in **fig. 2d-e**. The shape of the CV plotted in **fig. 2d** and **fig. 2e** is very different depending on the selected liquid electrolyte. On one hand, the CV plots measured in 1M KOH correspond to the typical signature of sputtered VN films[41,42,44] evaluated in potassium hydroxide electrolyte. A redox wave centered at ~ -0.65 V vs Hg/HgO (for low N_2 content) is typically observed for such electrode materials[36,47] and the rectangular shape voltamogramms are

characteristic of a pseudocapacitive charge storage mechanism occurring within VN films as demonstrated recently[43,47]. From the CV depicted in **fig. 2d**, we can observe a decrease of the capacity value (in $C.cm^{-3}$ and normalized with the VN thickness) vs the increase of the N_2 content, in agreement with a densification process as discussed previously. In ionic liquid electrolyte (**fig. 2e**), the CV shape is very different and no redox wave is observed within the selected window potential (0.1 – 0.8 V vs Ag QRE). Regarding the CV shape, the volumetric capacity seems to be lower than that of measured in 1M KOH. The charge of VN films in EMIM TFSI is depicted in **fig. 2f.** Not surprisingly, we observe the effect of the densification process with the increasing of the nitrogen content in the gas mixture. To validate this hypothesis, the ratio between the charges evaluated in two electrolytes is reported in **fig. 2g** vs the nitrogen content in the total gas. Again, we observe a decrease of the capacity values when the N_2 content is increased (densification process): both the pseudocapacitive and EDL contributions follow the same trend. Based on the electrochemical measurements achieved in EMIM TFSI, we observe that the double layer capacitance (DLC) varies from ~ 157 to ~ 26 $F.cm^{-3}$ for 10 and 100 % nitrogen content respectively (**fig. 2f**). Even if the double layer formation is different in these two electrolytes – KOH and EMIM TFSI – we have plotted the ratio between the charge in EMIM TFSI and the charge in 1M KOH in **Fig. 2g**. This ratio varies between 4 and 18% depending on the nitrogen in the gas mixture confirming the influence of the densification process. Similar observations (**fig. SI1e-f**) were done with another ionic liquid electrolyte ($BMIM^+TFSI^-$) while the size of the used cation ($BMIM^+$) is different than the one from $EMIM^+$.

The preliminary study reported in **fig. 2** and **fig. SI1** allows drawing some important conclusions regarding the effect of nitrogen flow rate on the VN properties. In depth electrochemical investigations (rate capability, cycling stability) in 1M KOH are

summarized in **fig. 3**. First, we measured the evolution of the volumetric capacitance at various scan rates in 1M KOH for different N_2 ratios. Cyclic voltammograms at 2 and 100 $mV.s^{-1}$ are shown in **fig. 3a-b** and **fig. SI2a-b**. At 2 $mV.s^{-1}$, the CV is well defined and the redox wave at ~ -0.65 V vs Hg/HgO progressively disappears with the increase of the N_2 content. A possible explanation could be associated to the densification process. Indeed, the number of electroactive sites coming from the vanadium oxide species[43] may be reduced between the VN columns owing to the densification process thus leading to a significant reduction of the solid / liquid interaction during the electrochemical analyses. From CV experiment, it is well known that the current follows a power law ($I_{peak} = av^b$). "I" represents the current (mA) while "v" is the scan rate in $mV.s^{-1}$. In this formula, "a" and "b" are defined as arbitrary coefficients, but the b-value allows discriminating the type of electrochemical process involved in the charge storage mechanism within the sputtered VN films. While a b-value close to 0.5 reflect a purely diffusion-limited process such as classically reported in battery-type material, capacitive or pseudocapacitive processes lead to a b-value close to 1. From **fig. SI2c-d**, we observe that, when the nitrogen content is tuned from 10 up to 100 %, the b-value moves from ~ 0.9 up to ~ 1 evidencing that the charge stored in the VN thin films arise from an electrochemical process that is not limited by solid-state diffusion. Nevertheless, the high electrical conductivity value of VN films at high N_2 content (see **fig. 2.b** and **fig. SI2e**) allowed reaching a purely capacitive process without limitation of the ions diffusion within the pseudocapacitive material. Indeed, at 100 $mV.s^{-1}$ (one complete cycle in 12 s), the volumetric capacitance of the VN deposited with N_2 content higher than 80 % is similar to that of obtained at lower scan rates (2 $mV.s^{-1}$). From rate capability point of view, working with sputtered VN films deposited with N_2 content > 80 % seems thus an attractive solution. The evolution of the volumetric capacitance vs

the scan rates (from 2 up to 100 $mV.s^{-1}$) for various N_2 content (10-100 %) is proposed in **fig. 3c**. We demonstrate that the volumetric capacitance values do not significantly vary when the sweep rate was set between 2 and 100 $mV.s^{-1}$ for the VN films (**fig. SI2e**) deposited at high N_2 content (> 80 %). The difference of performance between the films deposited with 10 or 30 % nitrogen content could be due to the contribution of the redox waves at ~ -1 V vs Hg/HgO. Indeed, this redox system at ~ -1V vs Hg/HgO is very dependent of the nitrogen flow as explained later in the paper. The various capacitance values obtained in **fig. 3c** for the samples deposited at different flow rate is exacerbated at 2 $mV.s^{-1}$ due to the contribution of this redox wave. This is not the case for films deposited with low N_2 content (< 30 %) where the volumetric capacitance is scan rate-dependent. It could be noticed that higher capacitance is obtained for VN films deposited at low N_2 content, in apparent contradiction with the previous assumption. To decide between these two statements, capacitance retention was evaluated in 1M KOH during 5000 cycles (at 25 $mV.s^{-1}$) for various VN films where we tuned the N_2 content in the plasma from 10 to 100 %. In **fig. 3d**, we observe on one hand that the capacitance retention is decreasing and low, between 65 and 80 %, when the nitrogen content is set at a “low” level ($N_2 \leq 50$ %). On the other hand, the retention of the initial capacitance is much better (capacitance retention > 90 % during 5000 cycles) when the nitrogen content within the VN films is higher than 80 %. This is consistent with the structural behavior of sputtered VN films where we observe that the deposition at high N_2 content corresponds to the formation of bulk VN powder. The films deposited at N_2 content = 100 % even exhibits a capacitance retention of 110 % after 5000 cycles. In that case, the capacitance progressively increases during the first 3000 cycles due to an “activation” process attributed to the progressive penetration of the aqueous electrolyte in dense VN films upon charge/discharge cycling. Once the

capacitance value of the VN films deposited at N_2 = 100 % reached a threshold (after ~ 4000 cycles), the capacitance seems to stay in a steady state. However, this gas ratio is not the optimal one, since, even if its capacity retention is the best, volumetric capacitance is significantly lower than that measured with 80 or 90 % gases ratio (see **fig1.c**).

In the previous part, we have demonstrated that the deposition at high N_2 content is a key issue for high rate capability and large cycling stability. A question arise concerning the ageing of such sputtered vanadium nitride films acting as an efficient electrode of MSC for long term applications. In the field of catalyst or electrochemical capacitor, it is indeed well known that particles based on transition metal nitride are surrounded by a thin transition metal oxide layer whose properties change with increasing time[49] to ambient atmosphere. Since pseudocapacitance[48] charge storage mechanism involves the surface or sub-surface layers of the active electrode material, the ageing effect of sputtered vanadium nitride films is an important issue that, to the best of the authors' knowledge, is totally unexplored. In that context, we have evaluated the performance of various VN films deposited at low and high nitrogen content. Main important results are depicted in **fig. 4**. The CVs of a 360 nm-thick VN film deposited at N_2 = 13 % (chosen as representative of low N_2 content) and measured in 1M KOH at 50 $mV.s^{-1}$ are shown in **fig. 4a**. The as-deposited VN film exhibits a box-like CV shape between -1 and -0.4 V vs Hg/HgO with a volumetric capacitance close to ~1100 $F.cm^{-3}$ at 50 $mV.s^{-1}$. This value translates into 660 $C.cm^{-3}$ over a 0.6V potential window. According to the density of the film (3.5 $g.cm^{-3}$), the gravimetric capacity reaches 189 $F.g^{-1}$ which corresponds to 0.12 electron per mole of VN, thus supporting our previous findings about the surface-limited charge storage in VN electrodes[43].

After 1 month, a similar analysis, in exactly the same electrochemical conditions, was conducted. Interestingly, the CV shape is totally different and exhibits a very resistive behavior, that we attribute to the ageing effect. We believe (this assumption will be discussed later in the next paragraph) that this effect could be due to the formation of a low conductive vanadium oxide films at the surface of the VN films. Similar experiments were performed on a 238 nm-thick VN film deposited at N_2 content = 90% (representative of high N_2 ratio) and the results are summarized in **fig. 4b**. At 50 $mV.s^{-1}$, the CVs of the as-deposited film is rectangular with a high volumetric capacitance close to ~ 950 $F.cm^{-3}$. The good electrical conductivity of sputtered VN film deposited at N_2 = 90% is responsible for this remarkable electrochemical performance at 50 $mV.s^{-1}$. The experiments were carried out in a similar way after 40 days, 2 months and 13 months and no ageing effect was observed. More specifically, the capacitance value was even a little bit higher after 13 months and stayed close to ~ 1000 $F.cm^{-3}$ at 50 $mV.s^{-1}$. The rate capability of the two VN films is shown in **fig. 4c** and **fig. SI3** at various scan rates. The VN film deposited at N_2 = 13% (blue curve) seems, at first sight, to be interesting when considering only the performance at 2 $mV.s^{-1}$ (volumetric capacitance = 1500 $F.cm^{-3}$ after 1 month of ageing). Nevertheless, the large difference in electrochemical performance between the as-deposited sample and after 1 month clearly showed that it is definitely not a good strategy for long-term applications based on efficient MSC. This is however not the case for the VN film deposited at N_2 = 90% where the performance stay at the same level of magnitude after 13 months of ageing in air. To verify the hypothesis regarding the formation of a low conductive layer of vanadium oxide (see previously), Raman spectroscopy analyses were carried out on the two sputtered vanadium nitride films deposited with low (~ 10%) and high N_2 (~ 90%) content (**fig. 4d**). Ageing effect are clearly observed on these two samples, where

the Raman spectra are significantly different when considering the VN film deposited with N_2 ~ 10% (as-deposited and aged sample). No well-defined peaks are observed on the Raman spectra of the pristine VN sample (black curve) and only a small peak at 520 cm^{-1} characteristic of the silicon substrate is highlighted. Three broad bands with low intensities (~ 234, 379 and 842 cm^{-1}) are pointed out with spectra similar to already published ones for VN films or VN slurry prepared by magnetron sputtering method or solution processing route respectively[50,51]. The Raman spectra acquired on the same samples (orange curve) after 10 months revealed the presence of a set of well-defined peaks (at 146, 262, 320, 411, 500, 690 and 990 cm^{-1} respectively) which could be ascribed to the presence of a surface oxide layer on VN[52] corresponding to the progressive oxidation of sputtered VN films. Regarding the literature[53], this surface oxide layer could probably correspond to an amorphous V_2O_5 film or a poorly crystallized α-V_2O_5. As the electrical conductivity of V_2O_5 is very low[54] (σ_{elec} ~ 6.5 x 10^{-6} $S.cm^{-1}$), we propose that this layer is responsible for the high resistive behavior of the CV plots observed for aged-sputtered VN films deposited with low N_2 content. In contrast, no ageing effect (after 1 year) was observed (pink and blue curves) on Raman spectra of “old” sputtered VN films deposited at high N_2 content, and the set of broad peaks is attributed to the VN film[50,55].

Finally, we have evaluated the cycling stability of two VN films deposited at high N_2 content (N_2 = 70 and 90 %) during 50 000 cycles in 1M KOH. This cycling stability study was coupled with the ageing one and the electrochemical performance was also measured after 13 months. As illustrated in **fig. 4e-f**, both the Capacitance Retention (CR) and the Coulombic Efficiency (CE) are better for the film deposited with the highest nitrogen content. Note also that the CR and the CE of the VN film deposited at N_2 = 90 % with 13 months of ageing were higher than 85 % and 98 %, respectively.

In summary, from the results reported in **fig. 2-4**, we demonstrate that, to exhibit high rate capability, high cycling stability and slow ageing while keeping good capacitance, it is mandatory to deposit VN films by magnetron sputtering method at high N_2 content in the total gas. In addition, in a previous study[43], we have recently demonstrated that the deposition pressure plays also a key role for maximizing the surface capacitance value of VN films by enabling a fine control of the film porosity. In that context, in the present study, we also tuned the deposition pressure (from 9.2 x 10^{-3} up to 10^{-2} mbar) while taking into account a high nitrogen content (N_2 > 80 %) in the total gas during the sputtering process, to stay in optimized operating conditions. X-Ray Diffraction analyses (**fig. SI4**) were firstly carried out on numerous VN films and several N_2 – pressure combinations (6 gas ratio and 3 deposition pressures giving rise to a total of 18 samples) were tested to select the VN film showing the best performance. We clearly see a strong evolution of the preferred orientation with both the pressure and the N_2 ratio, as already reported in the literature for tribological issues of VN coatings, not used for their electrochemical properties but for their attractive hardness properties[46,56]. The **fig. 5a** summarizes the evolution of the ratio between the intensity of the (111) vs the (200) Bragg peaks regarding the N_2 content in total gas and the deposition pressure. We observe that this ratio progressively decreases and converges toward the theoretical ratio issued from JCPDS card (VN powder, 36-0768) meaning that the VN film is approaching the VN bulk free powder behavior. It is the same tendency that was observed previously (for the N_2 ratio study) for the cell parameter evolution, i.e. that both preferred orientation effects and cell parameter variation tend to ideal δ-VN powder as referenced in the PDF file 36-0768. Detailed electrochemical analyses were also carried out on these samples. The CV plots measured at 2 mV.s^{-1} are shown in **fig. 5b**: as expected from our previous studies[42,43],

the deposition at high pressure should lead to a higher capacitance value for a fixed N_2 content. For instance, for a N_2 content fixed at 80 %, chosen as representative of high N_2 content, the volumetric capacitance moves from ~ 700 $F.cm^{-3}$ (pressure = 9.2 x 10^{-3} mbar) to ~ 900 $F.cm^{-3}$ (pressure = 10^{-2} mbar). From these CV, we observe a redox wave centered between -1 and -0.9 V vs Hg/HgO. This redox peak could correspond to hydrogen evolution of the aqueous electrolyte (H_2O electrolysis) or a redox system attributed to the vanadium nitride film. To answer this question, we enlarged the working potential window of the CV to set the lower limit of the potential window close to -1.1 V vs Hg/HgO. From **fig. 5c**, we can observe that this wave centered at ~ -1 V vs Hg/HgO can be attributed to a reversible redox reaction of vanadium oxides species, as already reported by Choi *et al* [36] and Morel *et al* [41]. As demonstrated recently[43], the selected deposition parameters for sputtered VN films induced a feather-like growth morphology where highly conductive vanadium nitride allowed the fast electron transfer and where the reversible reaction took place within a very thin film of vanadium oxide surrounding the VN scaffold. We have previously shown that the charge storage process in vanadium nitride films arises from a fast charge transfer reaction at the surface or sub-surface of a very thin layer of vanadium oxides. This reversible reaction corresponds to an oxidation state change of vanadium oxides from 3+ to 4+, and reversibly, when cycling in KOH aqueous electrolyte between -1 and -0.4 V vs Hg/HgO [43]. The involvement of V^{2+} (VO) or V^{5+} (V_2O_5) species can be ruled out as confirmed by XPS and *operando* X-Ray Absorption analyses[43]. We previously shown that vanadium oxides species (redox active materials) were localized between two feathers or two columns but we did not evaluate precisely the position of the V_2O_3 and VO_2 oxides within the VN film. In that context, we deeply investigate the vanadium nitride film deposited by sputtering technique on Si / Si_3N_4 substrate: the

feather like structure can be observed in **fig. 6a**, that displays a low magnification high-angle annular dark field (HAADF) of sputtered VN film. In order to obtain a detailed picture of the distribution of the vanadium oxides in the VN film, we have acquired two sets of electron energy-loss spectroscopy (EELS) spectrum-images (SIs) at the regions labeled “top” and “bottom” in **fig. 6a. Fig. 6b** displays a high-resolution transmission electron microscopy (HRTEM) image of such a region, where it can be observed that its inter-reticular distance nevertheless matches that of VN material (2.3 Å)**.** Most spectra in the datasets correspond to mixtures of different vanadium compounds. However, we have been able to identify spectra corresponding to pure vanadium oxide III (V_2O_3) and IV (VO_2) as displayed in **fig. 6c**. We could not identify regions of pure VN, since all VN spectra contained small amounts of oxygen (see “VN” spectrum in **fig. 6c**). This suggest the formation of a thin layer of oxide on top of VN during the deposition or as soon as the sample was in contact with air atmosphere. We also observe areas where the fine structure of the nitrogen K edge is markedly different from that of VN, and similar to the one observed in oxynitrides[57] (see “$V_xN_yO_z$” spectrum in **fig. 6c**). This indicates that the spectra pertains to oxynitride, rather than a mixture of VN and VO_2. The oxynitride V-$L_{3,2}$ fine structure is identical (at the energy resolution of the analysis, 1.8 eV) to that of VO_2. Hence, the oxidation state of vanadium is 4+. Oxynitride involving V^{3+} may also be present but, at the experiment’s resolution, it would be indistinguishable from a mixture of VN and V_2O_3. **Fig. 6d-e** display EELS bonding maps obtained by fitting fine structure fingerprints extracted from the spectra in **fig. 6c** to the top and bottom EELS-SIs sets. The shafts of the feathers are mainly composed of vanadium nitride. They have a thin layer of oxide at the surface. The columns get thinner, more porous and increasingly oxidized towards the edge of the feathers. The most marked difference between the “top” and “bottom”

regions is the amount of V_2O_3. The “bottom” region are V_2O_3-rich. However, the “top” region are chiefly VO_2-rich. We observe that the distribution of the nitrogen element in oxynitride is strongly correlated with that of VO_2. Therefore, either the majority of the V^{4+} is in the form of oxynitride, or oxynitride is always present at the interface between VN and VO_2. As discussed above, the same may be true for V^{3+}, but the present experiment cannot verify it.

Nevertheless, when the working potential window was enlarged down to -1.1 V vs HgO, a more pronounced reversible redox reaction occurring at ~ 1V vs Hg/HgO could be observed. At this potential and regarding the pH of the solution, we could assign this pair of redox peaks to the reversible reduction of V^{3+} to V^{2+} as proposed by Djire et al[47]. An alternative explanation can be the role of native hydrogen adatoms following the reduction of water molecules. Indeed, there are already some reports about hydrogen storage in VN films[58,59] and it can be envisioned that this reaction could be electrochemically driven prior to hydrogen evolution. Thus, reversible electrochemical hydrogen storage cannot be ruled out especially according to the potential at which the couple of redox peaks is observed (~ -1 V vs Hg/HgO). Such peculiar behavior will be investigated in a forthcoming study.

Consequently, it was mandatory to avoid this additional reaction, whatever its nature, and thus to push back the redox reaction outside the selected working window potential (-1 up to -0.4 V vs Hg/HgO) from cycling stability point of view: working pressure and nitrogen content in the total gas was tuned to reach this goal. We thus evaluated the shift of the redox wave position at 2 $mV.s^{-1}$ in 1M KOH vs the deposition pressure and the nitrogen content in the total gas. The results are summarized in **fig. 5d**. A set of unfavorable deposition conditions is visible from this experiment, i.e films with N_2 content lower than 91 % that induce, whatever the deposition pressures, the presence

of this redox wave within the selected working potential window. Nevertheless, we clearly see that this redox wave can be pushed back outside the working potential windows if the N_2 content is higher than 91 %. Among those favorable cases, three ratios were isolated at 10^{-2} mbar (91, 95 and 100%) and one at 9.6 10^{-3} mbar, 95% N_2. However, the electrical conductivity of VN films deposited at high deposition pressure is very low (~ 160 $S.cm^{-1}$). This is due to the induced porosity and thus a reduction of the rate capability of the films is observed. We finally compared the cycling stability of two VN films deposited at the same N_2 content (= 95 %) but at two deposition pressure. From the capacitance retention measurement illustrated in **fig. 5e**, we can conclude that the VN film deposited at 9.5 x 10^{-3} mbar exhibits the best capacitance retention value during 10 000 cycles. Those conditions (95% N_2 and a pressure of 9.5 x 10^{-3} mbar) are thus the optimal ones, considering all the compromises between good capacitance, ageing, rate capabilities and long cyclability.

Finally, if we consider a micro-supercapacitor's application rather than only the intrinsic properties of the electrode, we have to maximize the surface performance, taking into account a limited footprint surface. To reach this goal, a solution consists in the fabrication of electrodes with high thickness and high electrical conductivity. In that context, we have then to study the evolution of the surface capacitance value vs the thickness of sputtered VN films. Note however that, regarding the optimization made in the frame of this paper, we have also to study the cycling stability and the rate capability of the VN electrode.

We first evaluated the performance of thin VN film (76 nm-thick). The results were summarized in **fig. 7**. The cycling stability (**fig. 7a-b**) was remarkable with a capacitance retention of ~ 100 % during 150 000 cycles and a coulombic efficiency of 95 %. The CV plots of the 76 nm-thick VN film reported in **fig. 7b** at different cycle

numbers (500th, 10 000th, 75 000th and 125 000th cycles) illustrate the high cycling stability. Rate capability of the VN electrode was measured at various scan rates (**fig. 7c**): at 0.2 V.s^{-1} (one complete cycle in 6 s), the volumetric capacitance was ~ 400 F.cm^{-3} and only 25 % of this capacitance value was lost at 1.4 V.s^{-1} (one complete cycle in ~ 0.85 s) showing the ultra-high rate performance (**fig. 7d**). Then, we progressively increased the film thickness up to 32.2 µm (**fig. 8**). The surface capacitance value was evaluated vs the film thicknesses and the scan rates (from 2 up to 100 mV.s^{-1}). The results are reported in **fig. 8a-b**. At 2 mV.s^{-1}, we observe that the surface capacitance values are correlated with the film thickness: the maximum value reaches ~1.1 and 1.4 F.cm^{-2} for 15.8 and 32.2 µm-thick VN films made from magnetron sputtering process. Due to the optimization made on these films, this value only decreased down to 0.55 F.cm^{-2} when cycling at 100 mV.s^{-1} (time to make one charge/discharge cycle = 12 s) while it was a key issue to keep high the capacitance value for fast electrochemical microdevices[30]. More specifically, the rectangular shape fingerprint of pseudocapacitive material was kept at 10 mV.s^{-1} whatever the thickness as illustrated on the CV plots[48] from **fig. 8c**. Nevertheless, we observe (for 15.8 µm and 32.2 µm-thick films, **fig. 8b**) a limited-process coming from either ion diffusion limitation process or electron transport within the thick sputtered films[3]. Nevertheless, the maximum surface capacitance values (~ 1.4 F.cm^{-2}) is one of the best value reported up to now when considering a planar configuration where the electrode material was deposited as a film on flat substrate (here a silicon wafer). This value is compared regarding state of the art film electrodes made from deposition facility widely used in semiconductor industry. A 7 µm-thick carbon-derived carbide (CDC) film delivers only 0.1 F cm^{-2} in organic electrolyte[1,21]. In 1M H_2SO_4 electrolyte[1], 5 µm-thick CDC films deliver up to 0.2 F cm^{-2}. MXene Ti_3C_2-T electrode is an attractive solution

for MSC application while delivering both high areal and volumetric capacitance values. In that context, 5 µm-thick Ti_3C_2-T ‘‘clay’’ electrodes[60] deliver up to a 0.4 F cm^{-2} / 900 F cm^{-3} capacitance values when measured in 1 M H_2SO_4. Recent results on 3D electrode made from Laser-induced graphene scaffold coated with Ti_3C_2-T_x MXene film reported similar performance (~ 1.3 F.cm^{-2}) but using a two-step process for the electrode fabrication[61]. Finally, cycling stability measurement was achieved in 1M KOH at 50 mV.s^{-1} during 34 000 cycles and the cycling performance (CR and CE) of 8.7 µm-thick VN film was summarized in **fig. 8d**. Not surprisingly, the CE stayed close to 100 % while the CR is higher than 90 % after 34 000 cycles thus validated the selected strategy proposed in this paper. The CV plots reported in **fig. 8e** confirmed the high cycling stability of this sputtered VN film. The Nyquist plots of 8700 nm-thick sputtered VN film is shown in **fig. 8f**. The Electrochemical Impedance Spectroscopy measurement[62] was achieved at open circuit voltage after a stabilization in 1M KOH. We observe a quasi-vertical line in the low frequency region and a small semi-circle at high frequency. This semi-circle behaviour could be attributed to a charge transfer resistance of a pseudocapacitive electrode if the value of the resistance changes with the applied potential. If the resistance value stays constant with the applied potential, the semi-circle could be attributed to an interfacial contact resistance. As the value change with the applied working potential, we observe a charge transfer resistance coming from the pseudocapacitive behaviour of the VN film. From the equivalent circuit diagram (shown in **fig. 8f**) composed of an inductance (cable), a contact resistance, a second resistance in parallel with a Constant Phase Element (CPE, for modelling the charge transfer) and a second CPE for the capacitive contribution at low frequency (quasi vertical line), we extract the Equivalent Series Resistance (ESR ~ 1.04 ohm.cm^2) and the charge transfer resistance (R_{CT} = 0.21 ohm.cm^2). These very low

values clearly confirm the remarkable properties of the sputtered VN as a current collector and pseudocapacitive material for MSC. From the Nyquist plot (**Fig. 8f and SI5**), the real and imaginary parts of the surface capacitance were also extracted[31,63]. The relaxation time constant τ_0 = 1.47 s of VN electrode, given at the frequency where C″ is maximum (f = 0.68 Hz), is in good agreement with the expected value of such pseudocapacitive electrode[14,64]. The Galvanostatic Charge / Discharge plots of the 8.7 µm-thick VN sample are depicted in **fig. 8g-h** at different current densities. Not surprisingly, the GCD plots exhibit a triangular shape whatever the current densities revealing the pseudocapacitive behaviour of the VN electrodes in 1M KOH.

The charge storage mechanism of sputtered vanadium nitride films in 1M KOH was previously unveiled[43] in 2020 by our group using combined *operando* X-Ray absorption spectroscopy analyses with *in situ* Atomic Force Microscopy measurement and TEM / EELS analyses. Herein, we try to tackle the cycling stability issue which is a key point for transferring the technology to pilot production line. In that context, this paper clearly demonstrates the remarkable cycling, ageing and rate capability performance of sputtered vanadium nitride. Nevertheless, a question arises to explain the mechanism involved in VN films (showing a cubic structure) to reach such performance. On one hand, from XRD structural analyses reported in **fig. 2**, we observe that the evolution in the cell parameter follows a V-shape plot with a minimum value when the nitrogen content in the gas mixture was set to 20 – 40 % (see method section for the definition). In this case, the cell parameter value reached 4.112 Å, which is far from the theoretical one expected for a pure polycrystalline VN powder (4.139 Å). On the other hand, from electrochemical measurements, as reported in **fig. 3** and **4**, we demonstrated that a low nitrogen content in the gas mixture led to VN films with low capacitance retention (poor cycling stability) and in turn the ageing of such VN films

led to lower capacitance values. Moving from 20 – 40 % up to 90 - 100 % of nitrogen in the gas mixture allowed the cell parameter to converge or exceed the theoretical value (4.139 Å). Consequently, the sputtered VN film deposited with such high nitrogen content in the gas mixture exhibited the cell parameter of a bulk VN powder. From electrochemical point of view, the VN films deposited at high N_2 content in the gas mixture have demonstrated very nice cycling stability and no ageing effect. We can thus propose that to reach the highest cycling stability, it is better to deposit VN films with a cell parameter close to the theoretical value. In addition, when the nitrogen content in the gas mixture is too low, the sputtered VN films oxidized rapidly, with the formation of amorphous V_2O_5 film or poorly crystallized α-V_2O_5, as depicted by Raman analyses on **fig. 4**. In contrast, no ageing effect after 1 year was observed on the Raman spectra of sputtered VN films deposited with high N_2 content, meaning that the cubic structure of vanadium nitride films is fully saturated with nitrogen, leading to minor oxidation process when the films were in contact with air atmosphere even for a long period of time.

CONCLUSION

We demonstrate in the present manuscript that sputtered vanadium nitride films deposited with high nitrogen content are attractive candidates as pseudocapacitive electrodes for MSC applications. More specifically, this unexplored domain clearly confirmed that both the nitrogen content and the pressure have to be carefully controlled to produce VN electrode with high rate capability (> 1 $V.s^{-1}$), high cycling stability (> 150 000 cycles), very low ageing (after 13 months) and high surface capacitance value (~ 1.4 $F.cm^{-2}$). New finding regarding the localization of vanadium oxide species responsible for the pseudocapacitive behavior of sputtered vanadium nitride films is proposed. This paper brings new insights in the field of transition metal nitride films and opens the way toward the development of very stable electrode that could be suitable for powering the next generation of Internet of Things devices with micro-supercapacitors.

ACKNOWLEDGEMENT

The authors thank the French National Research Agency (STORE-EX Labex Project ANR-10-LABX-76-01 and ARTEMIS ANR-22-ASEN-0001 project) for financial support. The French RENATECH network and the University of Lille are greatly acknowledged for the supporting the Center of MicroNanoFabrication (CMNF) facility from IEMN. Chevreul Institute (FR 2638), Ministère de l'Enseignement Supérieur et de la Recherche, Région Hauts de France and FEDER are acknowledged for supporting and funding XRD and TEM facilities.

DATA AVALAIBILITY

The data that support the plots within this paper and other findings of this study are available from the corresponding authors upon reasonable request.

COMPETING INTERESTS.

The authors declare no competing interests.

MATERIALS & CORRESPONDENCE.

Correspondence to Christophe Lethien, Thierry Brousse & Pascal Roussel.

REFERENCES

[1] P. Huang, C. Lethien, S. Pinaud, K. Brousse, R. Laloo, V. Turq, M. Respaud, A. Demortière, B. Daffos, P. L. Taberna, B. Chaudret, Y. Gogotsi, P. Simon, *Science (80-.).* **2016**, *351*, 691.

[2] C. Lethien, J. Le Bideau, T. Brousse, *Energy Environ. Sci.* **2019**, *12*, 96.

[3] P. Simon, Y. Gogotsi, *Nat. Mater.* **2020**, *19*, 1151.

[4] H. K. Kim, T. Y. Seong, J. H. Lim, W. Cho, Y. Soo Yoon, *J. Power Sources* **2001**, *102*, 167.

[5] Y. S. Yoon, W. I. Cho, J. H. Lim, D. J. Choi, *J. Power Sources* **2001**, *101*, 126.

[6] X. Yu, J. B. Bates, J. G. E. Jellison, F. X. Hart, *J. Electrochem. Soc.* **1997**, *144*, 524.

[7] T. Pichonat, C. Lethien, N. Tiercelin, S. Godey, E. Pichonat, P. Roussel, M. Colmont, P. A. Rolland, *Mater. Chem. Phys.* **2010**, *123*, 231.

[8] M. Nisula, Y. Shindo, H. Koga, M. Karppinen, *Chem. Mater.* **2015**, *27*, 6987.

[9] N. A. Choudhury, S. Sampath, A. K. Shukla, *Energy Environ. Sci.* **2009**, *2*, 55.

[10] C. Zhong, Y. Deng, W. Hu, J. Qiao, L. Zhang, J. Zhang, *Chem. Soc. Rev.* **2015**, *44*, 7484.

[11] A. Guyomard-Lack, P. E. Delannoy, N. Dupré, C. V. Cerclier, B. Humbert, J. Le Bideau, *Phys. Chem. Chem. Phys.* **2014**, *16*, 23639.

[12] L. Negre, B. Daffos, V. Turq, P. L. Taberna, P. Simon, *Electrochim. Acta* **2016**, *206*, 490.

[13] M. F. El-Kady, R. B. Kaner, *Nat. Commun.* **2013**, *4*, 1475.

[14] M. F. El-Kady, M. Ihns, M. Li, J. Y. Hwang, M. F. Mousavi, L. Chaney, A. T. Lech, R. B. Kaner, *Proc. Natl. Acad. Sci.* **2015**, *112*, 4233.

[15] B. Asbani, B. Bounor, K. Robert, C. Douard, L. Athouël, C. Lethien, J. Le Bideau, T. Brousse, *J. Electrochem. Soc.* **2020**, *167*, 100551.

[16] M. Brachet, D. Gaboriau, P. Gentile, S. Fantini, G. Bidan, S. Sadki, T. Brousse, J. Le Bideau, *J. Mater. Chem. A* **2016**, *4*, 11835.

[17] C. Choi, K. Robert, G. Whang, P. Roussel, C. Lethien, B. Dunn, *Joule* **2021**, 1.

[18] P. E. Delannoy, B. Riou, B. Lestriez, D. Guyomard, T. Brousse, J. Le Bideau, *J. Power Sources* **2015**, *274*, 1085.

[19] D. Pech, M. Brunet, H. Durou, P. Huang, V. Mochalin, Y. Gogotsi, P.-L. Taberna, P. Simon, *Nat. Nanotechnol.* **2010**, *5*, 651.

[20] H. Durou, D. Pech, D. Colin, P. Simon, P. L. Taberna, M. Brunet, *Microsyst. Technol.* **2012**, *18*, 467.

[21] M. Létiche, K. Brousse, A. Demortière, P. Huang, B. Daffos, S. Pinaud, M. Respaud, B. Chaudret, P. Roussel, L. Buchaillot, P. L. Taberna, P. Simon, C. Lethien, *Adv. Funct. Mater.* **2017**, *27*, DOI 10.1002/adfm.201606813.

[22] B. E. Conway, in *Electrochem. Supercapacitors*, **1999**, pp. 259–297.

[23] S. Ardizzone, G. Fregonara, S. Trasatti, *Electrochim. Acta* **1990**, *35*, 263.

[24] S. Trasatti, G. Buzzanca, *J. Electroanal. Chem.* **1971**, *29*, 4.

[25] J. P. Zheng, P. J. Cygan, T. R. Jow, *J. Electrochem. Soc.* **1995**, *142*, 2699.

[26] M. Toupin, T. Brousse, D. Bélanger, *Chem. Mater.* **2004**, *16*, 3184.

[27] H. Y. Lee, J. B. Goodenough, *J. Solid State Chem.* **1999**, *144*, 220.

[28] A. Ferris, S. Garbarino, D. Guay, D. Pech, *Adv. Mater.* **2015**, *27*, 6625.

[29] K. Brousse, S. Pinaud, S. Nguyen, P. F. Fazzini, R. Makarem, C. Josse, Y. Thimont, B. Chaudret, P. L. Taberna, M. Respaud, P. Simon, *Adv. Energy Mater.* **2020**, *10*, 1.

[30] B. Asbani, G. Buvat, J. Freixas, M. Huvé, D. Troadec, P. Roussel, T. Brousse, C. Lethien, *Energy Storage Mater.* **2021**, *42*, 259.

[31] E. Eustache, C. Douard, A. Demortière, V. De Andrade, M. Brachet, J. Le Bideau, T. Brousse, C. Lethien, *Adv. Mater. Technol.* **2017**, *2*, 1.

[32] A. Ferris, D. Bourrier, S. Garbarino, D. Guay, D. Pech, *Small* **2019**, *15*, DOI 10.1002/smll.201901224.

[33] B. Bounor, B. Asbani, C. Douard, F. Favier, T. Brousse, C. Lethien, *Energy Storage Mater.* **2021**, *38*, 520.

[34] Q. Jiang, N. Kurra, M. Alhabeb, Y. Gogotsi, H. N. Alshareef, *Adv. Energy Mater.* **2018**, *8*, DOI 10.1002/aenm.201703043.

[35] B. Asbani, K. Robert, P. Roussel, T. Brousse, C. Lethien, *Energy Storage Mater.* **2021**, *37*, 207.

[36] D. Choi, G. E. Blomgren, P. N. Kumta, *Adv. Mater.* **2006**, *18*, 1178.

[37] T. -C. Liu, W. G. Pell, B. E. Conway, S. L. Roberson, *J. Electrochem. Soc.* **1998**, *145*, 1882.

[38] J. Shi, B. Jiang, C. Li, F. Yan, D. Wang, C. Yang, X. Wang, Z. Liu, *Surf. Coatings Technol.* **2021**, *405*, 126535.

[39] S. Ouendi, K. Robert, D. Stievenard, T. Brousse, P. Roussel, C. Lethien, *Energy Storage Mater.* **2019**, *20*, 243.

[40] A. Achour, R. L. Porto, M. A. Soussou, M. Islam, M. Boujtita, K. A. Aissa, L. Le Brizoual, A. Djouadi, T. Brousse, *J. Power Sources* **2015**, *300*, 525.

[41] A. Morel, Y. Borjon-Piron, R. L. Porto, T. Brousse, D. Bélanger, *J. Electrochem. Soc.* **2016**, *163*, A1077.

[42] K. Robert, C. Douard, A. Demortière, F. Blanchard, P. Roussel, T. Brousse, C. Lethien, *Adv. Mater. Technol.* **2018**, *3*, 1.

[43] K. Robert, D. Stiévenard, D. Deresmes, C. Douard, A. Iadecola, D. Troadec, P. Simon, N. Nuns, M. Marinova, M. Huvé, P. Roussel, T. Brousse, C. Lethien, *Energy Environ. Sci.* **2020**, *13*, 949.

[44] E. Le Calvez, D. Yarekha, L. Fugère, K. Robert, M. Huvé, M. Marinova, O. Crosnier, C. Lethien, T. Brousse, *Electrochem. commun.* **2021**, *125*, 107016.

[45] Q. Wei, R. H. DeBlock, D. M. Butts, C. Choi, B. Dunn, *Energy Environ. Mater.* **2020**, *3*, 221.

[46] J. H. Huang, C. H. Lin, G. P. Yu, *Thin Solid Films* **2019**, *688*, 137415.

[47] A. Djire, P. Pande, A. Deb, J. B. Siegel, O. T. Ajenifujah, L. He, A. E. Sleightholme, P. G. Rasmussen, L. T. Thompson, *Nano Energy* **2019**, *60*, 72.

[48] T. Brousse, D. Belanger, J. W. Long, *J. Electrochem. Soc.* **2015**, *162*, A5185.

[49] O. Kartachova, Y. Chen, R. Jones, Y. Chen, H. Zhang, A. M. Glushenkov, *J. Mater. Chem. A* **2014**, *2*, 12940.

[50] N. Fateh, G. A. Fontalvo, G. Gassner, C. Mitterer, *Tribol. Lett.* **2007**, *28*, 1.

[51] R. Manjunatha, A. Karajić, H. Teller, K. Nicoara, A. Schechter, *ChemCatChem* **2020**, *12*, 438.

[52] C. M. Ghimbeu, E. Raymundo-Piñero, P. Fioux, F. Béguin, C. Vix-Guterl, *J. Mater. Chem.* **2011**, *21*, 13268.

[53] P. Shvets, O. Dikaya, K. Maksimova, A. Goikhman, *J. Raman Spectrosc.* **2019**, *50*, 1226.

[54] C. Sanchez, R. Morineau, J. Livage, *Phys. Status Solidi* **1983**, *76*, 661.

[55] L. Aissani, A. Alhussein, C. Nouveau, L. Ghelani, M. Zaabat, *Surf. Coatings Technol.* **2019**, *378*, DOI 10.1016/j.surfcoat.2019.124948.

[56] L. Aissani, M. Fellah, A. H. Chadli, M. A. Samad, A. Cheriet, F. Salhi, C. Nouveau, S. Weiß, A. Obrosov, A. Alhussein, *J. Mater. Sci.* **2021**, *56*, 17319.

[57] F. Hofer, P. Warbichler, A. Scott, R. Brydson, I. Galesic, B. Kolbesen, *J. Microsc.* **2001**, *204*, 166.

[58] A. Goncharov, A. Guglya, A. Kalchenko, E. Solopikhina, V. Vlasov, E. Lyubchenko, *J. Nanotechnol.* **2017**, *2017*, DOI 10.1155/2017/4106067.

[59] V. Bryk, A. Guglya, A. Kalchenko, I. Marchenko, Y. Marchenko, E. S. Melnikova, V. Vlasov, E. Zubarev, *OALib* **2015**, *02*, 1.

[60] M. Ghidiu, M. R. Lukatskaya, M. Q. Zhao, Y. Gogotsi, M. W. Barsoum, *Nature*

2015, *516*, 78.

[61] Y. Lei, W. Zhao, Y. Zhu, U. Buttner, X. Dong, H. N. Alshareef, *ACS Nano* **2022**, *16*, 1974.

[62] T. S. Mathis, N. Kurra, X. Wang, D. Pinto, P. Simon, Y. Gogotsi, *Adv. Energy Mater.* **2019**, *9*, DOI 10.1002/aenm.201902007.

[63] P. L. Taberna, P. Simon, J. F. Fauvarque, *J. Electrochem. Soc.* **2003**, *150*, A292.

[64] T. Dinh, F. Mesnilgrente, V. Conedera, N. A. Kyerematenq, D. Pech, *J. Electrochem. Soc.* **2015**, *162*, A2016.

[65] F. de la Peña, E. Prestat, V. T. Fauske, P. Burdet, J. Lähnemann, P. Jokubauskas, T. Furnival, M. Nord, T. Ostasevicius, K. E. MacArthur, D. N. Johnstone, M. Sarahan, J. Taillon, T. Aarholt, V. Migunov, A. Eljarra, J. Caron, C. Francis, T. Nemoto, T. Poon, S. Mazzucco, N. Tappy, N. Cautaerts, S. Somnath, T. Slater, M. Walls, F. Winkler, Håkon Wiik Ånes, **2022**, DOI 10.5281/zenodo.7090040.

[66] M. R. Keenan, P. G. Kotula, *Surf. Interface Anal.* **2004**, *36*, 203.

[67] R. Arenal, F. de la Peña, O. Stéphan, M. Walls, M. Tencé, A. Loiseau, C. Colliex, *Ultramicroscopy* **2008**, *109*, 32.

[68] A. Gloter, V. Serin, C. Turquat, C. Cesari, C. Leroux, G. Nihoul, *Eur. Phys. J. B* **2001**, *22*, 179.

METHODS

Preparation of the vanadium nitride films. Prior to the VN deposition, a Si_3N_4 layer (100 nm-thick) was deposited by a low-pressure chemical vapor deposition method (LPCD) at 800 °C (flow rates: 60 sccm for NH_3 and 20 sccm for SiH_2Cl_2) to protect the silicon wafer from the etching of the liquid electrolyte (1M KOH). VN films were prepared by DC-reactive magnetron sputtering of a pure 4" vanadium target (99.9 %) in an Alliance Concept CT200 reactor. Before the deposition, the pressure was kept below 10^{-6} mbar and the target-substrate distance was fixed at 6 cm. The power density and the temperature were fixed, respectively, 1.85 W cm^{-2} and 300 K. The deposition pressure and the nitrogen to argon ratio were modified so as to tune the film properties. The nitrogen content in the total gas or the gas mixture was evaluated taking into account the N_2 and Ar flow rate (nitrogen content (%) = N_2 / (N_2 + Ar) x 100). Different thicknesses were obtained depending on the deposition time.

Morphological and chemical analyses of VN films. Structural properties were examined by X-ray diffraction using a Rigaku Smarlab diffractometer in Bragg-Brentano mode employing Cu Kα-radiation (λ = 1.5418 Å). An offset of 2° was applied on the silicon substrate to avoid the high intensity of the (100) silicon peak. A Zeiss Ultra 55 scanning electron microscope (SEM), an atomic force microscope (AFM Dimension 3100) and a microbalance from Mettler Toledo XP6U were used to determine the morphology (cross section and top view analyses) of the films (thickness, roughness and density).

The FIB was performed using a dual-beam Thermo-Fisher Strata DB235 workstation. The electron beam source is a field emission gun and for the ion beam source, a liquid/metal gallium was used. Before the thin foil extraction, the selected areas were protected with Pt layer. The extraction has been performed in two steps. At the

beginning a beam current of about 10 nA at 15 kV was used. For the final thinning, a beam current of approximately 50 pA at 5 kV. This procedure was used in order to minimize amorphization, redeposition, and obtain homogeneous thickness of the studied regions. The high angle annular dark field (HAADF) images and STEM-EELS observations of thin foils extracted by focused ion been (FIB) were performed on a Thermo-Fisher TITAN Themis S/TEM microscope.

The TITAN Themis S/TEM microscope is equipped with a high brightness Schottky field emission gun, probe aberration corrector and monochromator (not used for this experiment), allowing spatial resolution of 65 pm and energy resolution of 150 meV. The microscope is also equipped with several annular dark field (ADF) detectors and a Quantum ERS/966 GIF with Dual EELS for quasi-simultaneous acquisition of low and high energy losses. The HAADF images on the Titan Themis were acquired with a convergence semi-angle of 21 mrad, 0.5 nm probe size, 100 pA beam current and a camera length allowing collection angles between 50 and 200 mrad. The STEM-EELS spectra images were acquired in spectrum image mode, with an entrance aperture of 2.5 mm and collection semi-angle of 49 mrad. An energy dispersion of 0.25 eV/channel was used to cover an energy range of about 500 eV in order to include N-K, V-$L_{3,2}$ and O-K edges. The energy resolution was 1.8 eV full-width half-maximum. Two spectrum images with size 356x64 pixel were acquired with 1.74 nm/pixel step and at 50 ms dwell time.

The analysis of the EELS datasets was performed with HyperSpy[65]. The low-loss and core-loss SIs were aligned using the low-loss SI as reference. In order to improve the signal-to-noise ratio of the core-loss SIs to enable fine structure analysis we process them with singular value decomposition thresholding weighted to account for Poisson

noise[66]. The threshold was chosen at six components based on inspection of the scree plot. HyperSpy's curve fitting features were used to perform the bonding analysis. Since standards for the compounds in the sample were not available, we extract the fine structure fingerprints from the datasets under analysis using a procedure similar to ref[67]. First, we fitted a single gaussian function to the V-L_3 white line to obtain maps of its centre, which is related to the element's oxidation state. Using this information, we identify spectra of two pure compounds, namely vanadium oxide III (V_2O_3) and vanadium oxide IV (VO_2). The identification was performed based on comparison with spectra in the literature[68] and on XPS and *operando* X-Ray Absorption analyses[43]. While the main material of the sputtered films is VN, all spectra of VN in the datasets contained small amounts of oxygen. The fact that, nonetheless, the interreticular distance measured by HRTEM corresponds to VN (see fig. 6b) indicate that it could be due to a thin layer of oxide at the surface of the sample. Additionally, we observe changes in the fine structure of N-K, that suggest the formation of oxynitrides[57]. Fig 6.c displays the four different spectra from which we have extracted the fine structure fingerprints. In particular, we have extracted O-K and V-$L_{3,2}$ fingerprints from the spectra labelled VO_2 and V_2O_3; N-K and V-$L_{3,2}$ fingerprints from the VN spectrum and N-K fingerprints from the $V_xN_yO_z$ spectrum. Notice that the V-$L_{3,2}$ and O-K fine structure of $V_xN_yO_z$ is very similar to that of VO_2 while its N-K fine structure is different from that of VN. We quantified the spectra using hydrogenic cross-sections and convolution with the low-loss to account for plural scattering. To estimate the fingerprint of pure VN from our slightly oxidized reference we incorporate the previously computed fingerprint of VO_2 in the model. For the bonding analysis of the Sis, we construct a model with a linear combination of all the fingerprints convolved with the low-loss and a power law function to account for the background. Finally, we

fit it to the noise-reduced SIs using a Levenberg-Marquardt algorithm with positive bounds on the ionization edges intensity. The intensity of those edges, in atoms per nanometre square, is displayed in fig. 6d-g.

Electrochemical characterizations. The Si / Si_3N_4 / VN sample was assembled as the working electrode in a flat cell designed by Biologic: the sample was sandwiched between a top and a bottom cells and the sealing was ensured by O-rings. A large cavity was drilled in the top cell allowing to fill the cavity with ~1 mL of liquid electrolyte. The contribution of the double layer capacitance provide by the VN films was evaluated in pure ionic liquid (EMIM TFSI and BMIM TFSI) and the electrochemical measurement was achieved in a glove box with controlled atmosphere (O_2 and H_2O quantities: less than 1 ppm). All the other electrochemical analyses were carried out oustside the glovebox in 1M KOH electrolyte. The O-ring's diameter defines the surface test of the VN films (0.4 cm^2). The electrochemical analyses of the VN films were carried out by cyclic voltammetry and electrochemical impedance spectroscopy measurement with a VMP3 potentiostat/galvanostat (Biologic) using a conventional three-electrode setup. The reference and the counter electrodes were Hg/HgO and a platinum wire, respectively when tested in 1M KOH electrolyte. VN thin films were cycled between -1 V and -0.4 V vs Hg/HgO according to the suitable conditions [41] proposed by D. Bélanger *et al*. A silver (Ag) wire was used as the quasi reference electrode when the electrochemical characterizations were achieved in ionic liquid electrolyte instead of a Hg/HgO reference electrode. The capacitance, in Farad (F) (or the capacity, in coulomb (C)) was extracted from the CV plots and the surface capacitance or capacity (in $F.cm^{-2}$ or $C.cm^{-2}$) was calculated taking into account the footprint surface delimited by the O-ring (0.4 cm^2). The volumetric capacitance (in $F.cm^{-3}$) or capacity (in $C.cm^{-3}$) were evaluated by divided the surface capacitance (capacity) values by the thickness

of the VN film. The surface capacitance (C, $F.cm^{-2}$) was calculated according to the following equation:

$$C = \frac{\int I dt}{S \Delta V} \qquad \text{Eq. 1}$$

where I is the current (A), S represents the footprint area (0.4 cm^2) and ΔV is the cell voltage (V).

Thanks to the high electronic conductivity of the VN layer, the films were used as a bi-functional material, thus acting both as the working electrode and the current collector.

LIST OF THE FIGURES AND FIGURE CAPTIONS

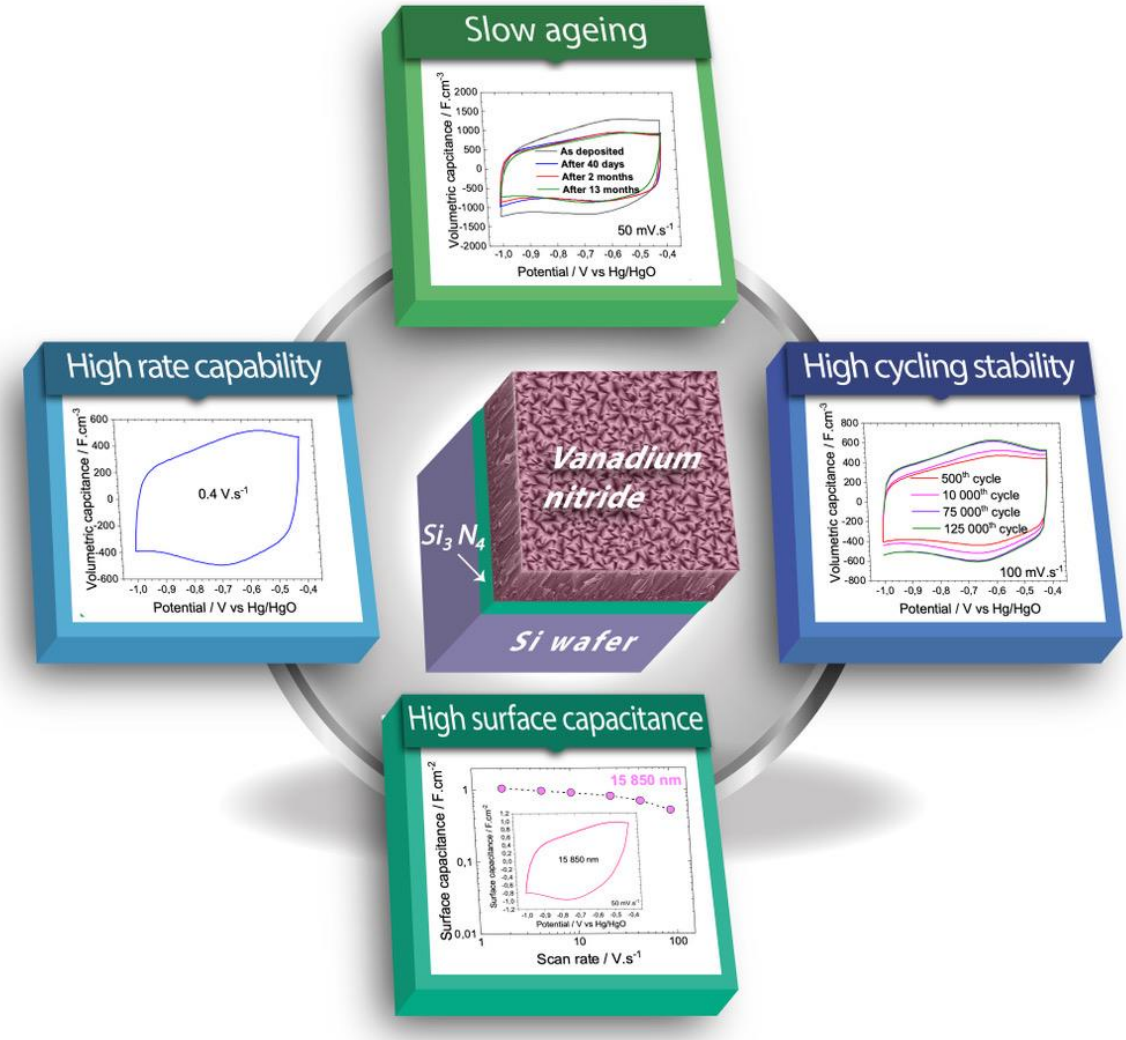

Fig. 1 | Overview of the proposed strategy to tune the ageing, cycling stability and rate capability of sputtered vanadium nitride films.

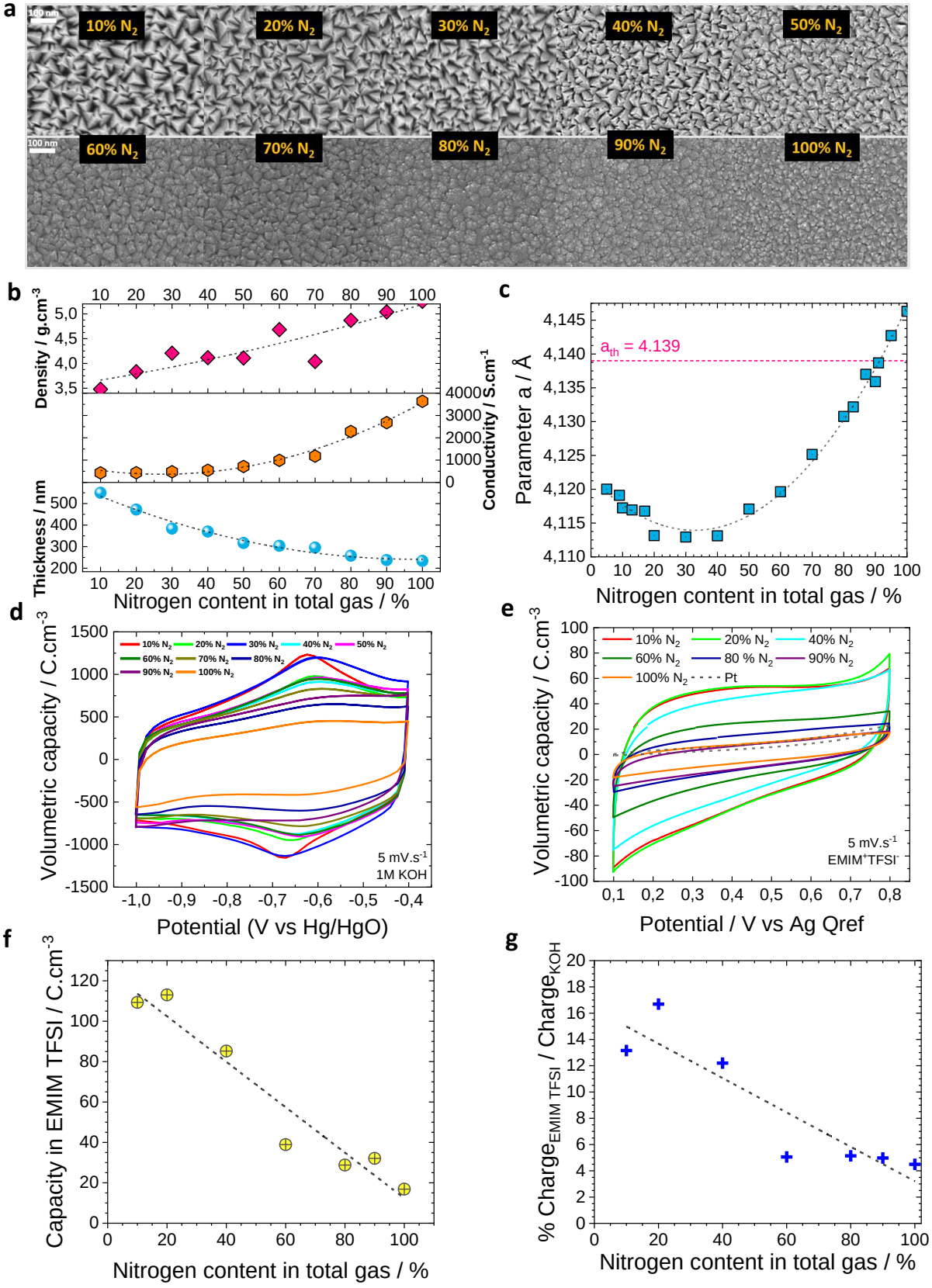

Fig. 2 | a. SEM analyses (top view) of the VN films deposited at various gas ratio. **b.** Evolution of the film density, electrical conductivity and thickness with the N_2 flow. **c.**

Evolution of the lattice parameter (a in Å) vs the nitrogen content in the total gas. **d.** Cyclic voltammetry plots of various VN films with different nitrogen content tested in 1M KOH aqueous electrolyte at 5 $mV.s^{-1}$. **e.** Cyclic voltammetry plots of various VN films with different nitrogen content tested in pure ionic liquid (EMIM-TFSI) at 5 $mV.s^{-1}$. **f.** Evaluation of the volumetric capacity in EMIM TFSI. **g**. Evaluation of the ratio between the capacity measured in 1M KOH and in EMIM TFSI ionic liquid electrolyte at 5 $mV.s^{-1}$.

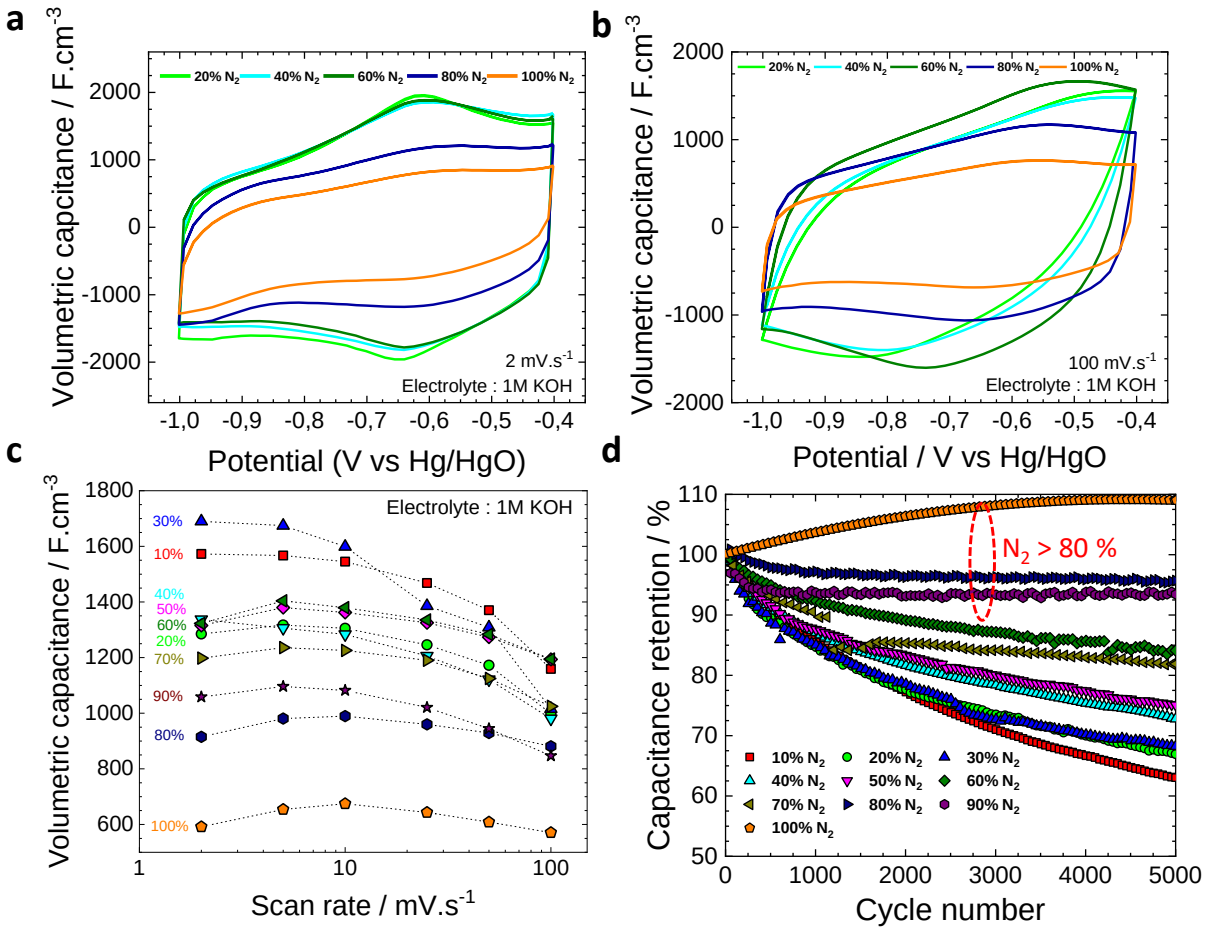

Fig. 3 | Electrochemical properties of the VN films vs the N2 content in the total gas. a-b. CV plots of the VN films evaluated in 1M KOH at 2 and 100 mV.s^{-1}. **c.** Evaluation of the volumetric capacitance vs the scan rates for various gas ratio. **d.** Capacitance retention evaluated during 5000 cycles at 25 mV.s^{-1}.

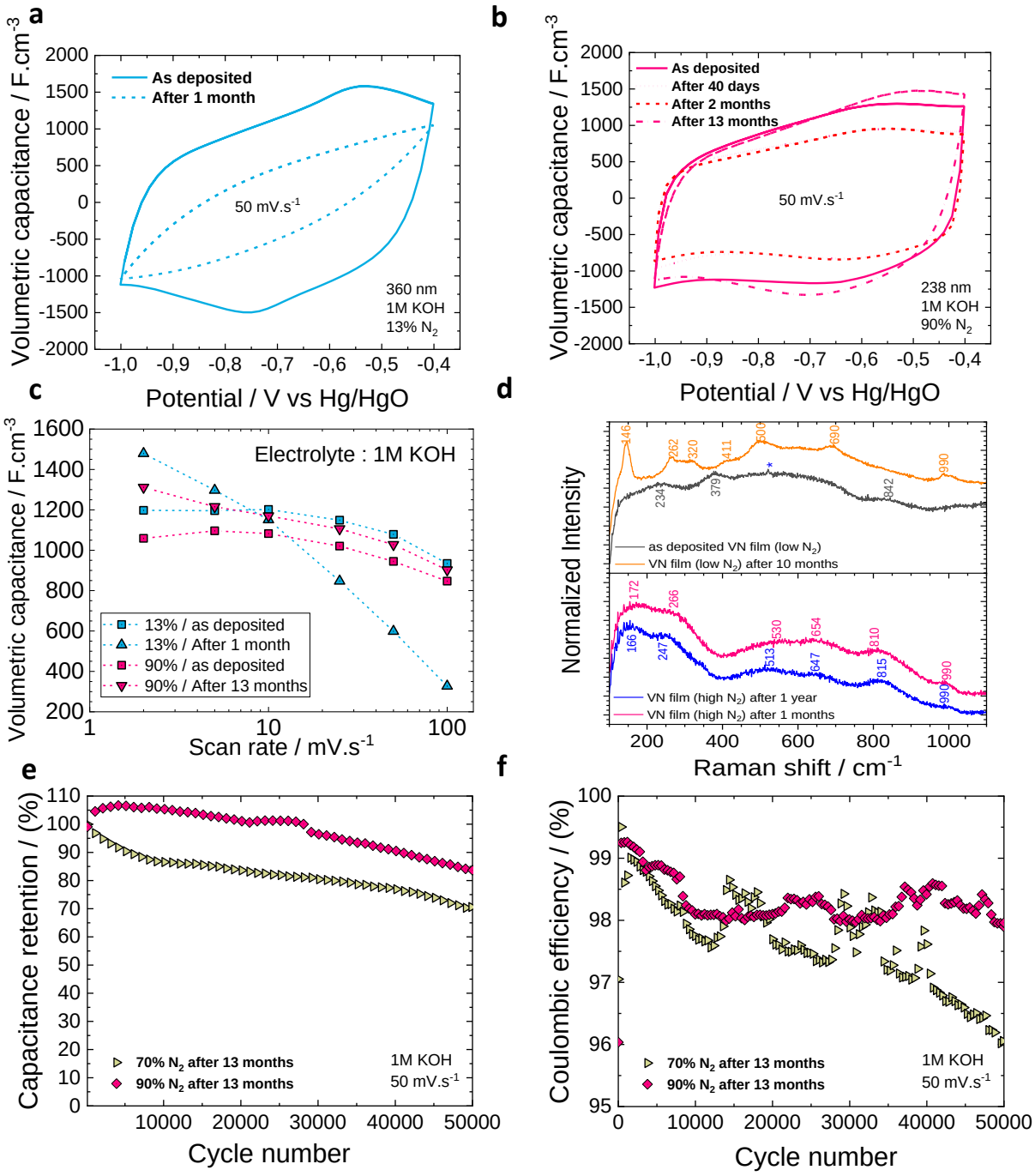

Fig. 4 | Ageing of the pseudocapacitive films in 1M KOH. a. CV plots at 50 mV.s^{-1} of sputtered VN films (13 % N_2): comparison of as-deposited sample and after 1 month. **b.** CV plots at 50 mV.s^{-1} of sputtered VN films (90 % N_2): comparison of as-deposited sample and after 40 days, 2 months and 13 months. **c.** Evolution of the volumetric capacitance value vs scan rate (13 % vs 90 % N_2). **d.** Raman analyses of two vanadium nitride films with low (~ 10 %) and high N_2 (~ 90 %) content (before and after ageing).

e-f. Capacitance retention and coulombic efficiencies of sputtered VN films deposited with two gas ratio (N_2 content = 70 % vs 90 %)

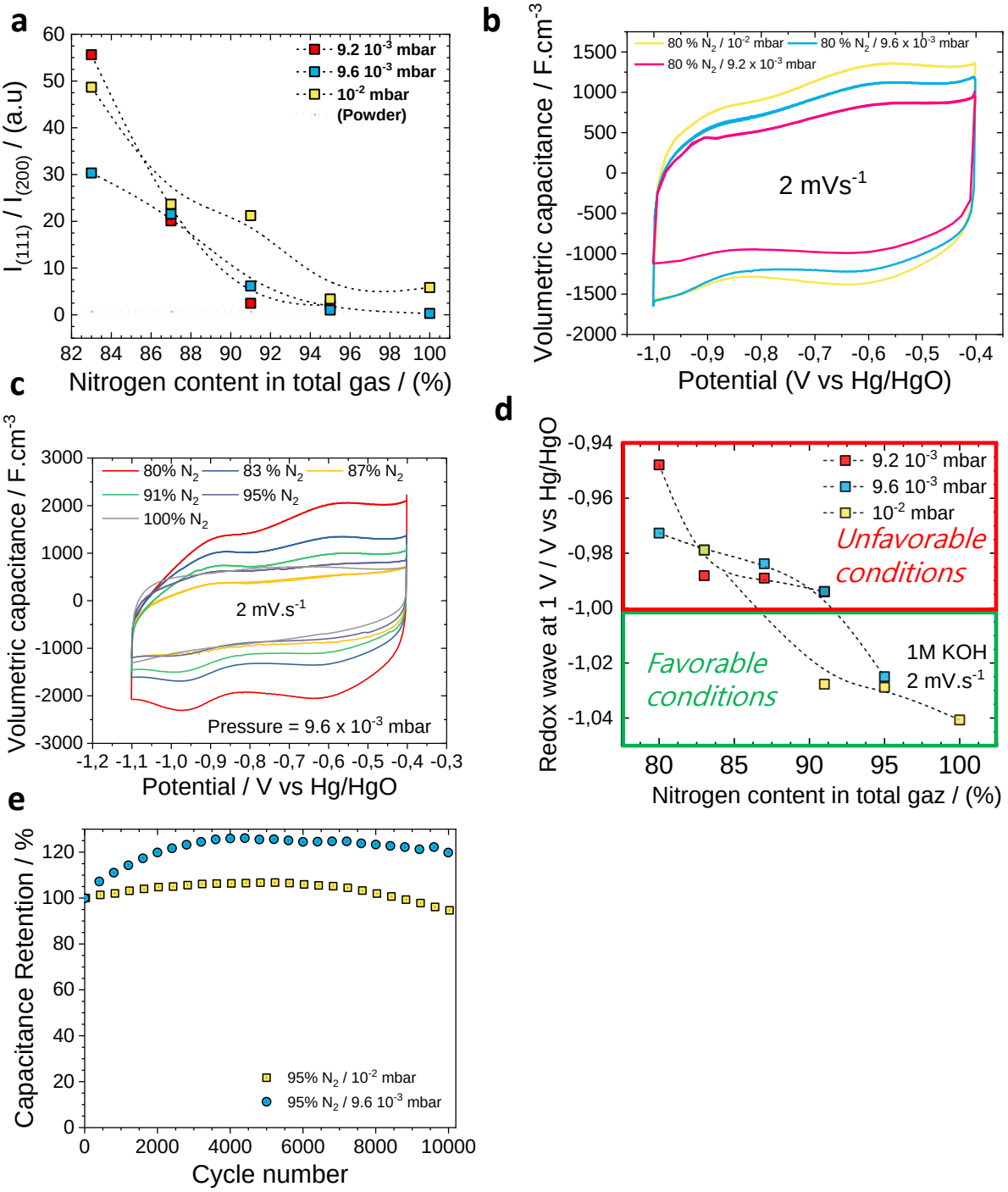

Fig. 5 | Tuning the film properties vs the nitrogen content in total gas and the deposition pressure. a. Evolution of the preferential orientation within the VN films vs the nitrogen total gas and the pressure. The range of the nitrogen content was restricted from 80 up to 100 % from stability point of view while the pressure was tuned from 9.2 x 10^{-3} up to 10^{-2} mbar. **b.** CV plots in 1M KOH (at 2 mV.s^{-1} and between -1

and -0.4 V vs Hg/HgO) of various VN films deposited with nitrogen content close to 80 % but at 3 different pressures. **c.** CV plots in 1M KOH (at 2 $mV.s^{-1}$ and between -1.1 and -0.4 V vs Hg/HgO) of various VN films deposited with different nitrogen content but at 9.6 x 10^{-3} mbar. **d.** Evaluation of the potential of the redox wave at ~ 1 V vs Hg/HgO regarding the N_2 content and the pressure. **e.** Cycling stability of the VN sample deposited with 95 % of N_2 and at two different pressure.

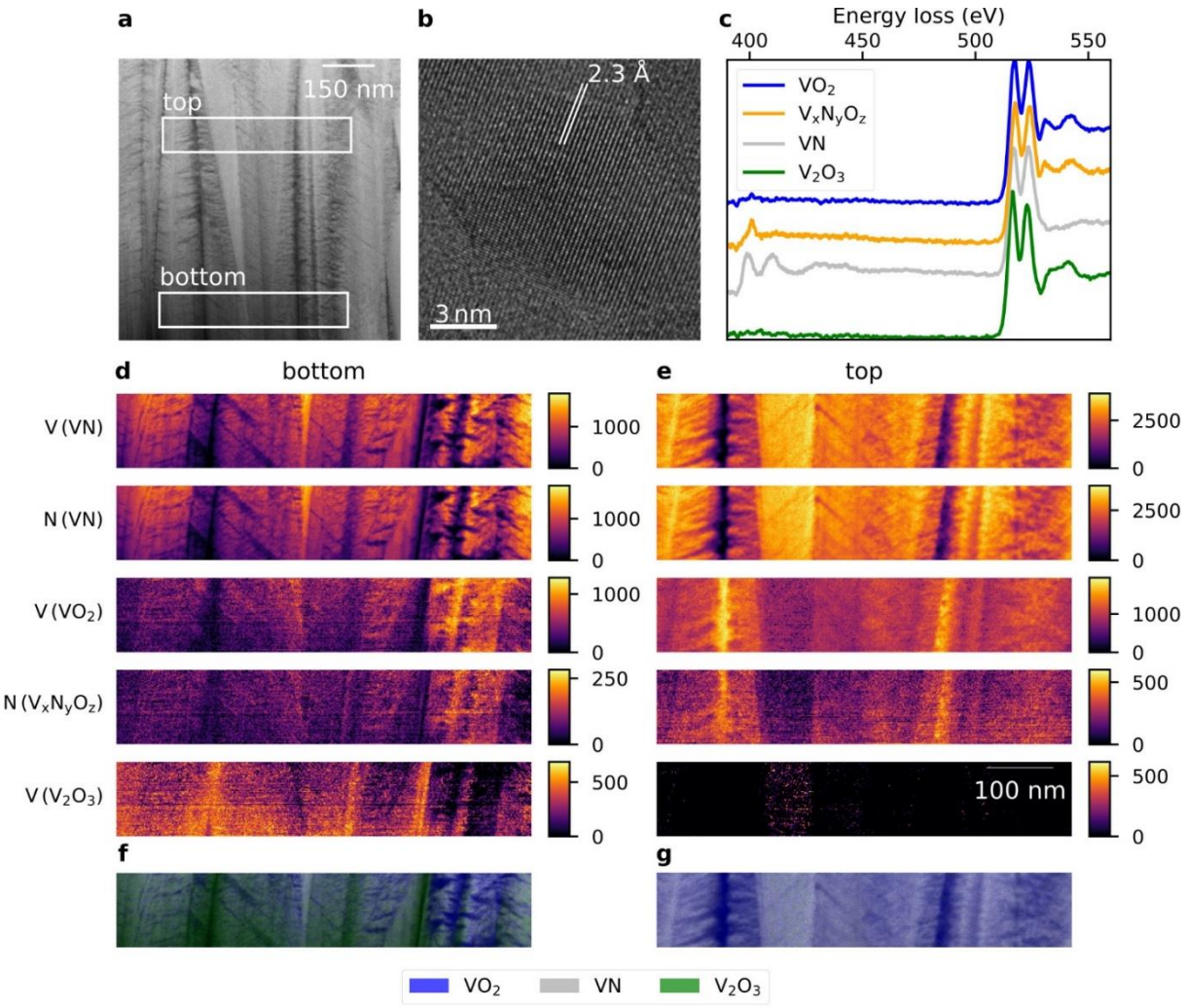

Fig. 6 | TEM – EELS analyses on sputtered vanadium nitride films. a. Low magnification HAADF of the sample with markers showing the two spectrum-images acquisition regions. **b.** HRTEM image of crystallized domains showing the 111 inter-reticular distance of VN. **c.** Reference spectra of vanadium oxide IV (blue), oxynitride (orange), vanadium nitride (silver) and vanadium oxide III (green), extracted from the spectrum images. The VN reference spectrum contains a small amount of oxygen. **d, e.** Bonding maps obtained by curve fitting of fine structure fingerprints extracted from the reference spectra in c. The color bar units are atoms per nanometer square. **f, g.** Color overlays of the VO_2, VN and V_2O_3 bonding maps above**.**

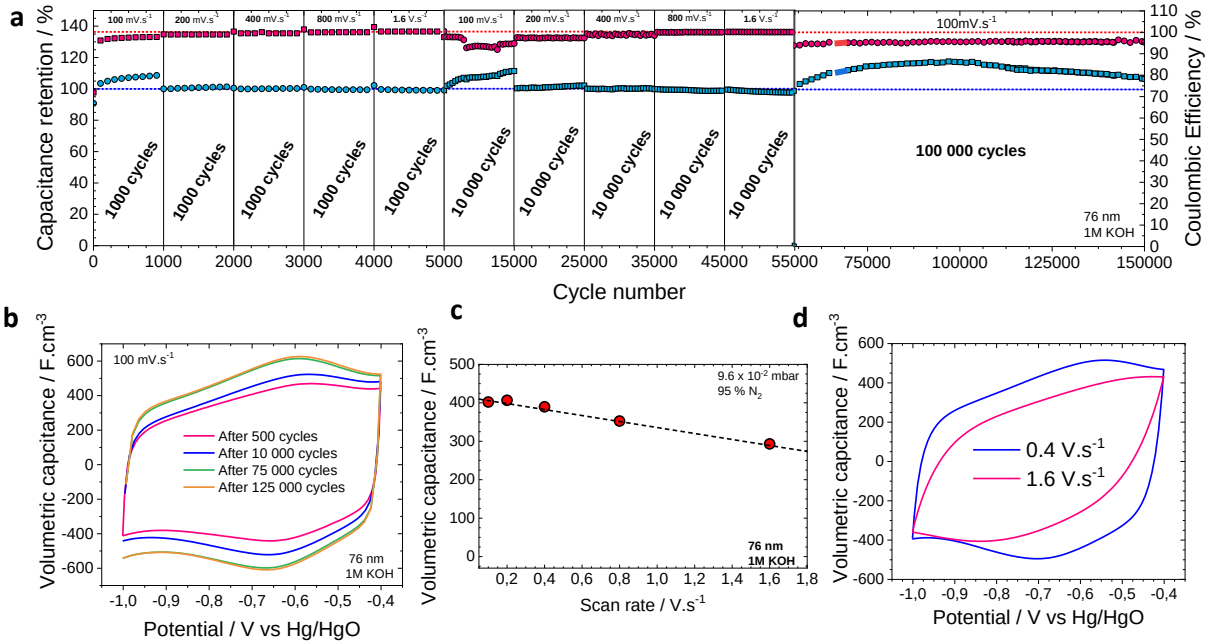

Fig. 7 | Evaluation of the cycling stability and rate capability of 76 nm-thick sputtered VN film in 1M KOH. a. Capacitance retention and coulombic efficiency of VN film evaluated during 150 000 cycles at different scan rates. **b.** CV plots of the 76 Nm-thick VN film at 100 mV.s^{-1} after 500, 10 000, 75 000 and 125 000 cycles. **c.** Rate capability of the electrode from 0.2 up to 1.6 V.s^{-1}. **d.** CV plots measured at 0.4 and 1.6 V.s^{-1} in 1M KOH.

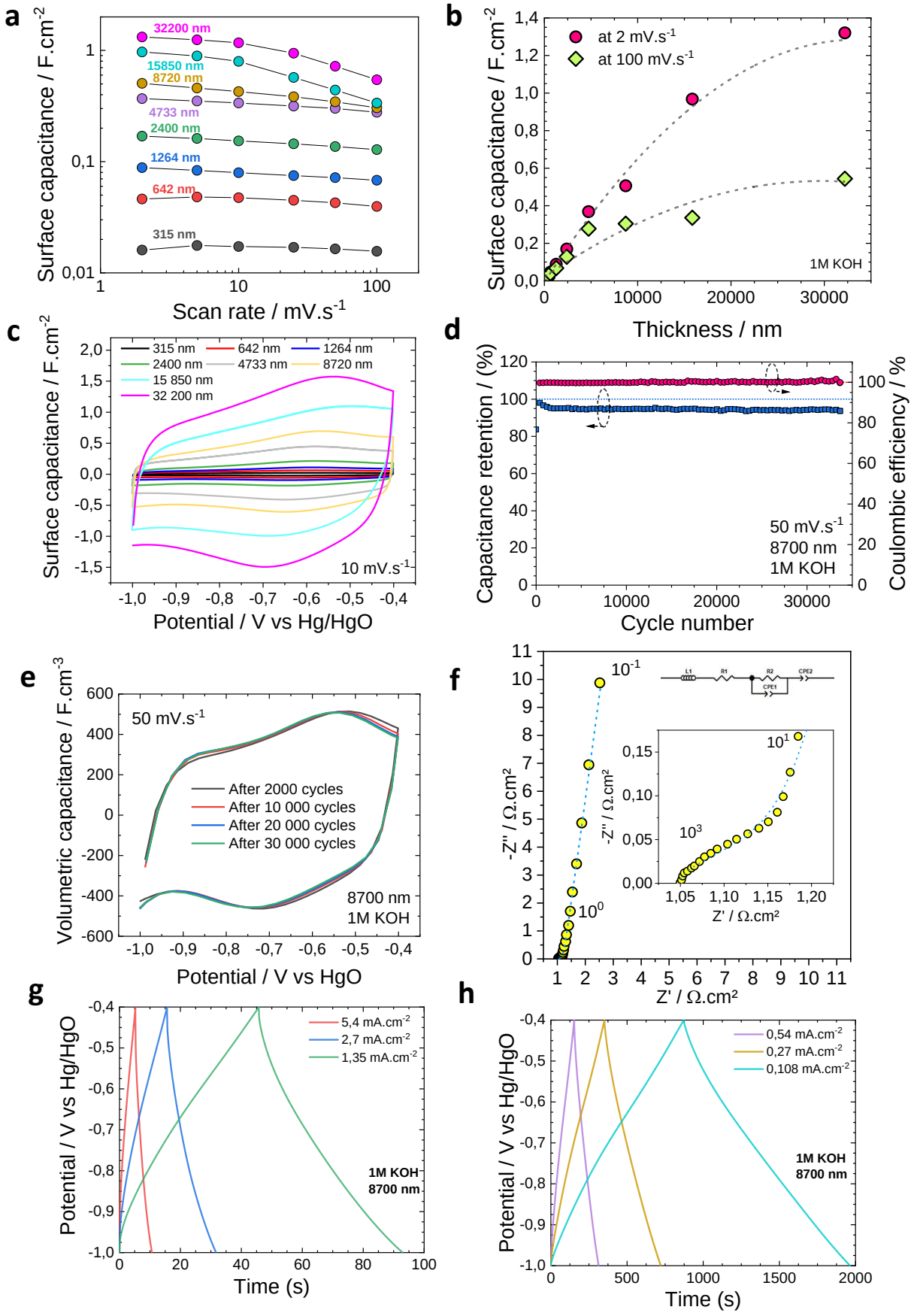
a
Surface capacitance / F.cm-2
Scan rate / mV.s-1
32200 nm
15850 nm
8720 nm
4733 nm
2400 nm
1264 nm
642 nm
315 nm
b
Surface capacitance / F.cm-2
Thickness / nm
at 2 mV.s-1
at 100 mV.s-1
1M KOH
c
Surface capacitance / F.cm-2
Potential / V vs Hg/HgO
315 nm
642 nm
1264 nm
2400 nm
4733 nm
8720 nm
15 850 nm
32 200 nm
10 mV.s-1
d
Capacitance retention / (%)
Coulombic efficiency / %
Cycle number
50 mV.s-1
8700 nm
1M KOH
e
Volumetric capacitance / F.cm-3
Potential / V vs HgO
50 mV.s-1
After 2000 cycles
After 10 000 cycles
After 20 000 cycles
After 30 000 cycles
8700 nm
1M KOH
f
-Z'' / Ω.cm²
Z' / Ω.cm²
10-1
100
101
103
g
Potential / V vs Hg/HgO
Time (s)
5,4 mA.cm-2
2,7 mA.cm-2
1,35 mA.cm-2
1M KOH
8700 nm
h
Potential / V vs Hg/HgO
Time (s)
0,54 mA.cm-2
0,27 mA.cm-2
0,108 mA.cm-2
1M KOH
8700 nm

Fig. 8 | Electrochemical performance of sputtered VN films vs the thickness of the electrode. a. Evaluation of the surface capacitance value of numerous VN films vs the scan rate from 2 to 100 $mV.s^{-1}$. **b.** Surface capacitance values vs the film thickness at 2 and 100 $mV.s^{-1}$ respectively **c.** CV plots of the various VN films at 10 $mV.s^{-1}$. **d.** Capacitance retention and coulombic efficiency of 8700 nm-thick VN film evaluated during 34 000 cycles. **e.** CV plots of the 8700 nm-thick VN film at 50 $mV.s^{-1}$ after 2000, 10 000, 20 000 and 30 000 cycles. **f.** Electrochemical Impedance Spectroscopy measurement evaluated in 1M KOH at open circuit voltage after stabilization. The model used to make the fit of the plot in depicted in the figures. **g-h.** Galvanostatic Charge / Discharge plots of 8700 nm-thick VN film at different current densities in 1M KOH.